JOURNAL OF THE ROYAL SOCIETY Interface

Oxygen mass transfer in a model three-dimensional artery

G Coppola and C Caro

J. R. Soc. Interface 2008 **5**, 1067-1075
doi: 10.1098/rsif.2007.1338

JOURNAL OF THE ROYAL SOCIETY Interface

J. R. Soc. Interface (2008) **5**, 1067–1075
doi:10.1098/rsif.2007.1338
Published online 5 February 2008

Oxygen mass transfer in a model three-dimensional artery

G. Coppola and C. Caro*

Department of Bioengineering, Imperial College London, London SW7 2AZ, UK

Arterial geometry is commonly non-planar and associated with swirling blood flow. In this study, we examine the effect of arterial three-dimensionality on the distribution of wall shear stress (WSS) and the mass transfer of oxygen from the blood to the vessel wall in a U-bend, by modelling the blood vessels as either cylindrical or helical conduits. The results show that under physiological flow conditions, three-dimensionality can reduce both the range and extent of low WSS regions and substantially increase oxygen flux through the walls. The Sherwood number and WSS distributions between the three-dimensional helical model and a human coronary artery show remarkable qualitative agreement, implying that coronary arteries may potentially be described with a relatively simple idealized three-dimensional model, characterized by a small number of well-defined geometric parameters. The flow pattern downstream of a planar bend results in separation of the *Sh* number and WSS effects, a finding that implies means of investigating them individually.

Keywords: artery; flow; oxygen; wall shear stress; blood–wall mass transport

1. INTRODUCTION

Arteries, as living tissues, require a supply of metabolites, including oxygen, and the removal of waste products. Oxygen is soluble in and reacts at the arterial wall, and its transport between the blood and the wall is reported to be controlled by the fluid phase rather than the wall (Tarbell 2003). Local oxygen lack in arterial walls (local hypoxia) has been proposed as contributing to the preferred occurrence of both atherosclerosis and intimal hyperplasia in low wall shear regions (Tarbell 2003); the former disease causes heart attack and stroke and the latter causes obstruction of arterial bypass grafts, vascular access grafts and endovascular stents. The underlying mechanisms are unclear, but hypoxia causes leakiness of the endothelium, and endothelial permeability to large molecules is increased in low wall shear regions (Himburg *et al.* 2004). Possible causes of these changes are effects of low wall shear stress (WSS) on apoptosis, or programmed death, of endothelial cells (Dimmeler *et al.* 1996), or on the expression of proteins associated with cellular permeability (Himburg *et al.* 2004).

Many groups have attempted to characterize arterial geometry and flow (Caro *et al.* 1971, 1996; Frazin *et al.* 1990; Stonebridge & Brophy 1991; Stonebridge *et al.* 1994; Long *et al.* 2000; Wood *et al.* 2006; O'Flynn *et al.* 2007). However, the limited availability of detailed *in vivo* data has made it necessary to draw heavily on model studies. Such studies infer that there will be strong secondary motion, cross mixing, a relatively uniform distribution of wall shear and suppression of flow separation, flow instability and flow stagnation (Caro *et al.* 1996, 1998, 2006; Friedman & Ding 1998).

*Author for correspondence (c.caro@imperial.ac.uk).

There has been recognition of the contribution of wall shear to the transport of low-molecular-weight species between the blood and the arterial wall (Caro *et al.* 1971; Tarbell 2003). However, molecular diffusion is a slow process compared with the distance over which mass transport must occur, which may be as much as the radius of a vessel. Therefore, mixing generated by secondary flow can be expected to enhance the transport of oxygen between the blood and the vessel wall (Caro *et al.* 2006). The flow in helical conduits is determined by the pitch and amplitude of the helix, and the flow rate and the physical nature of the fluid (Reynolds number). Depending on these quantities, there may be swirling and/or cross mixing (Liu & Masliyah 1993; Zabielski & Mestel 1998).

In this work, we study computationally the effect of cross mixing on oxygen transport between the blood and the vessel wall and on the distribution of WSS, by comparing the findings in two well-defined geometries, a cylindrical and a helical U-bend. We show that the helical geometry can capture the essential features of real vessels, like the coronary arteries, providing at the same time a simpler framework for understanding the effect of the geometrical parameters of the vessels. It may be noted that a helical geometry is relevant to certain U-shaped arteriovenous shunts (Caro *et al.* 2005) and vascular access grafts (Huijbregts *et al.* 2007).

2. METHODS

2.1. Computational domain and model

Two geometries were investigated: cylindrical is indicated as model 1 (figure 1*a*) and helical as model 2 (figure 1*b*,*c*). The first model is two-dimensional or

Received 15 December 2007
Accepted 16 January 2008

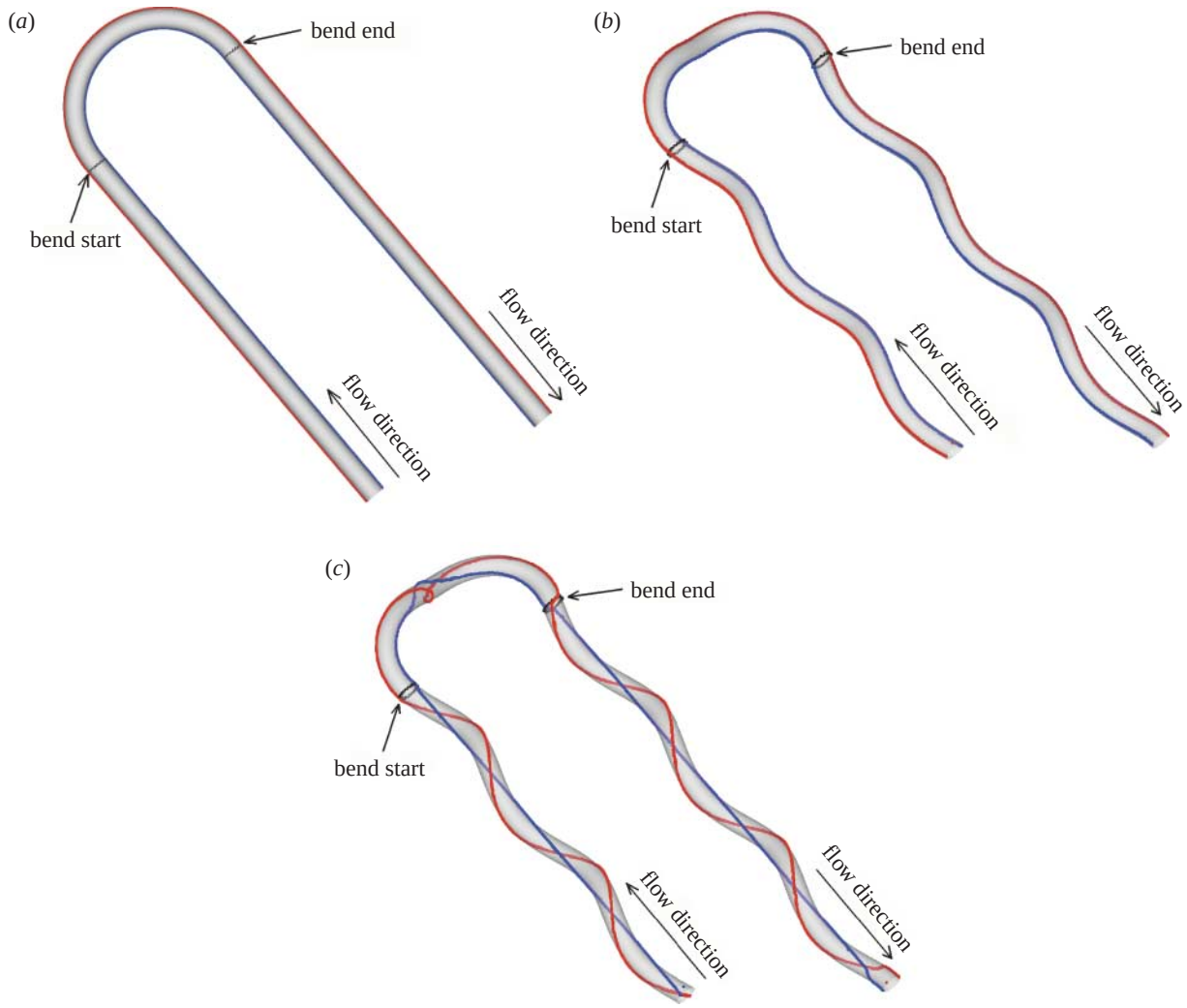

Figure 1. (*a*) Model 1: outer wall line (red) and inner wall line (blue). (*b*) Model 2: outer wall line based on primary curvature (red) and inner wall line based on primary curvature (blue). (*c*) Outer wall line based on secondary curvature (red) and inner wall line based on secondary curvature (blue). The flow direction and the bend start and end sections are indicated.

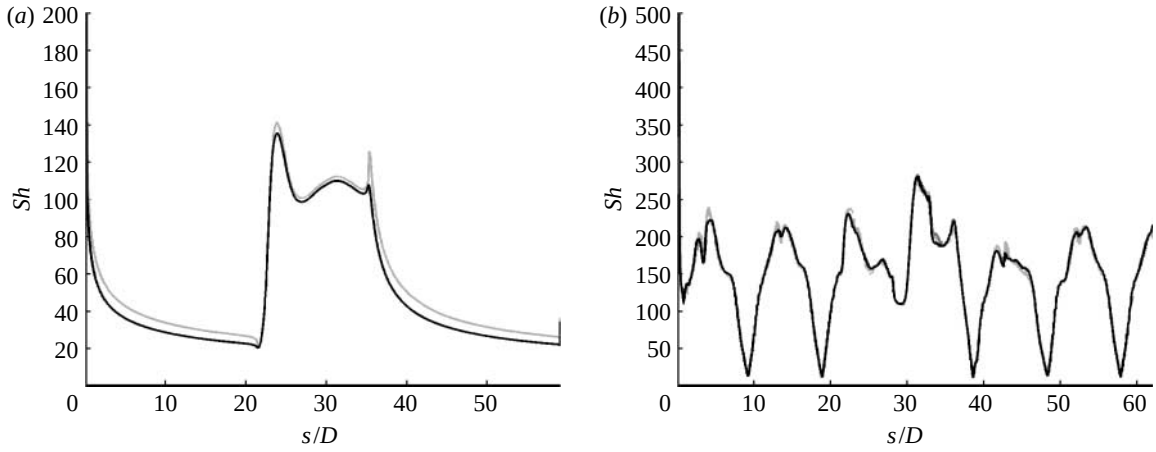

Figure 2. *Sh* number distributions at the outer wall lines (primary curvature) of (*a*) model 1 (light grey curves, 935 550 elements; dark grey curves, 1 104 400 elements; black curves, 1 608 408 elements) and (*b*) model 2 (light grey curves, 769 008 elements; dark grey curves, 1 749 320 elements; black curves, 2 480 560 elements), for three grids with different numbers of elements. The axial position is normalized by the vessel diameter.

planar, in the sense that its centreline is in a plane, while the second is three-dimensional, as its centreline is three-dimensional. The primary curvature (Kaazempur-Mofrad & Ethier 2001; Myers *et al.* 2001) is the curvature relative to the medial plane, while the secondary curvature (Kaazempur-Mofrad & Ethier 2001; Myers *et al.* 2001; Tiwari *et al.* 2006) is the curvature relative to the centreline. The wall lines

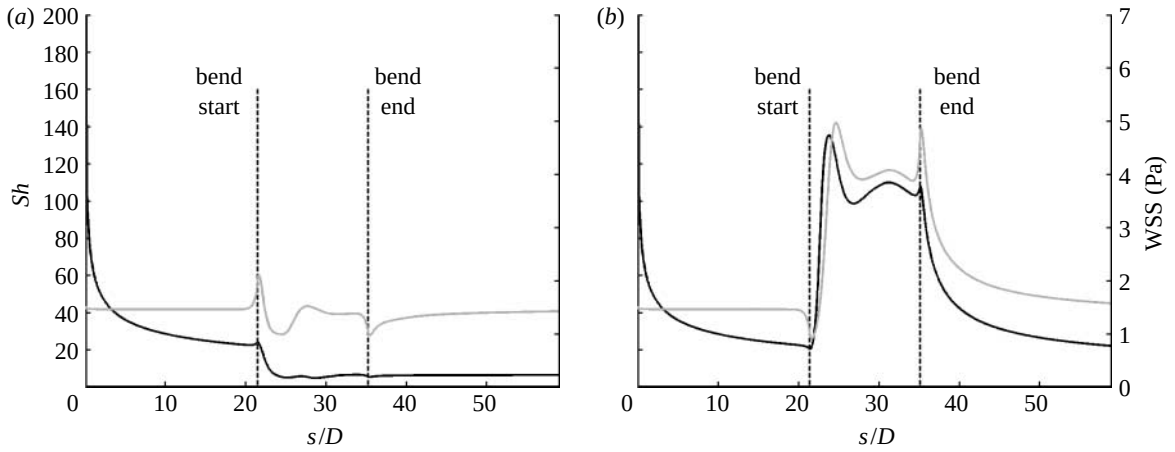

Figure 3. *Sh* number (black curves) and WSS (grey curves) distributions along (*a*) the inner and (*b*) outer wall lines (primary curvature) of model 1. The axial distance from the inlet is normalized by the vessel diameter. The dashed lines indicate the beginning and the end of the bend.

relative to the primary curvature are the lines resulting from the intersection of the projection (onto the medial plane) of the local normal to the centreline with the model surface. The wall lines relative to the secondary curvature result from the intersection of the local normal to the centreline with the model surface. In either case, the inner line is always on the side of positive curvature, while the outer one is on the negative side of it. These lines are reported in figure 1*a*,*b* for models 1 and 2, respectively, where red is the outer wall line and blue is the inner wall line. The inflexion in the wall lines based on the secondary curvature near the exit section of model 2 (figure 1*c*) is a geometric artefact, but does not affect our results. In model 1, the primary and secondary curvatures coincide. Both models have an internal diameter $D_i = 6$ mm. In model 1, the length of the section upstream of the bend $L_u \sim 21 D_i$, the length of the section downstream of the bend $L_d = 24 D_i$ and the radius of curvature of the bend $R_c \sim 4 D_i$. In model 2, $L_u \sim 20 D_i$, $L_d = 26 D_i$ and $R_c \sim 4 D_i$. The helix is defined by the pitch, $P = 55$ mm and the amplitude, $R_h = 0.5 D_i$.

The results were checked for mesh independence, by running simulations on three grids for each model: 935 550, 1 104 400 and 1 608 408 hexahedral elements for the first model and 769 008, 1 749 320 and 2 480 560 hexahedral elements for the second model. Convergence was assessed on the WSS and Sherwood number distributions on the inner and outer wall lines relative to the primary curvature, as shown in figure 2, where, for brevity, only the *Sh* number distribution is reported. The distributions are almost indistinguishable for the two meshes with a higher number of elements, leading us to conclude that adequate convergence had been achieved.

In both the models, the mass transport boundary layer was resolved by placing the first three grid nodes at 7.6, 9 and 10.8 μm away from the wall. The three-dimensional steady incompressible Navier–Stokes equations were solved with the finite volume-based commercial package FLUENT v. 6.0 (Fluent, Inc.). The SIMPLE formulation was used for pressure–velocity coupling, and the second-order upwind discretization scheme was used for the momentum and species transport equation. Convergence was achieved when the maximum mass, momentum and species residuals fell below 10^{-12}.

2.2. Flow conditions

The flow was assumed to be steady and the wall was rigid and stationary. Newtonian behaviour was assumed for the blood, with density $\rho = 1050$ kg m^{-3} and viscosity $\mu = 0.0035$ kg m^{-1} s. It was assumed, as also by several previous workers (Qiu & Tarbell 2000; Kaazempur-Mofrad & Ethier 2001; Perktold *et al.* 2002; Kaazempur-Mofrad *et al.* 2005; Tada & Tarbell 2006), that oxygen is present only in dissolved form in the plasma, with diffusivity $D_{O_2} = 1.2\,10^{-9}$ m^2 s^{-1}, giving a Schmidt number $Sc = \nu / D_{O_2} \sim 2800$. A typical physiological WSS in human arteries $\tau_{wf} \sim 1.5 \pm 0.5$ Pa (Malek *et al.* 1999). WSS affects the blood vessels in numerous ways: where the WSS rises above τ_{wf} throughout their length, the blood vessels may remodel, increasing in diameter until the WSS returns to the optimal value (Kamiya *et al.* 1984). If the WSS drops below τ_{wf} blood vessels may also reduce in size (Langille & O'Donnell 1986) and also in a localized area, such as a recirculation region, the vessel in that region may become vulnerable to disease (Caro *et al.* 1971; Giddens 1995). It is proposed that the WSS must fall to approximately 0.5 Pa (Malek *et al.* 1999; Palumbo *et al.* 2002) to favour the development of atherosclerosis, but the association between WSS and atherosclerosis may also depend on other factors, such as diet, blood lipid levels, hypertension, diabetes and smoking. A direct relationship between WSS, τ_w and Re can be derived by assuming a straight cylindrical shape for a model artery and fully developed flow, and after simple manipulations, one can easily get

$$Re = \tau_w \frac{\rho}{8\mu^2} D_i^2, \tag{2.1}$$

where $Re = \rho U D_i / \mu$, D_i is the vessel diameter and U is the inlet average velocity. From (2.1), for a 6 mm artery, the range of physiological $Re \in [390,770]$; in this

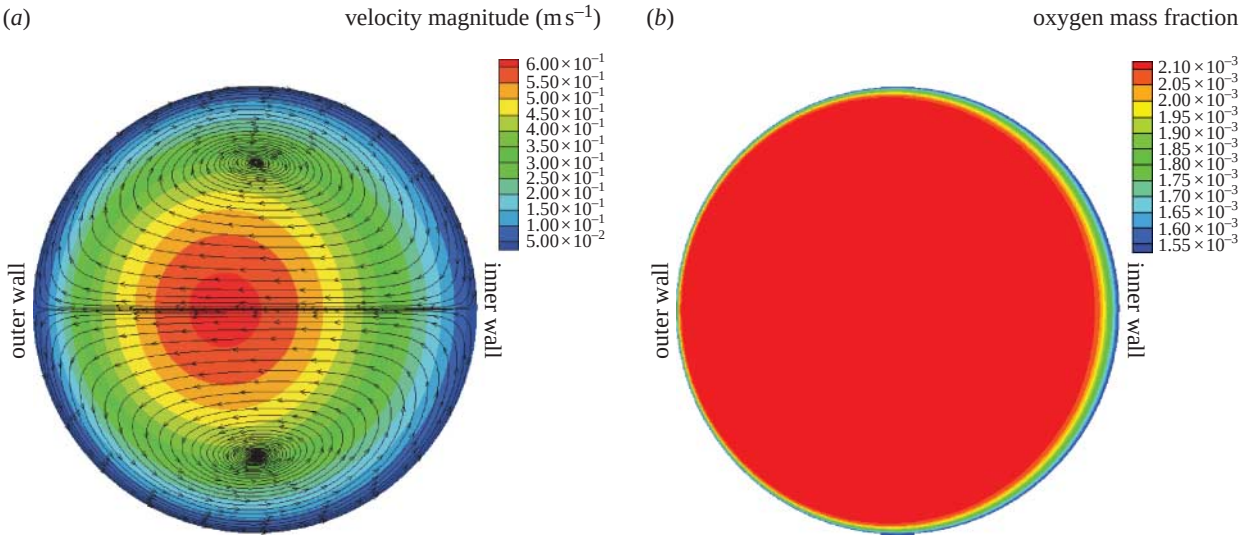

Figure 4. (*a*) Velocity magnitude iso-contours and in-plane streamlines; (*b*) oxygen iso-contours at a section 23*D* from the inlet in model 1 (approx. 1*D* in the bend). The inner and outer walls are also indicated.

work, we investigated one flow condition at $Re \sim 600$, well within the physiological range of *Re*.

Fully developed flow and a uniform inlet oxygen mass fraction, $y_i = 0.002125$, were imposed at the inlet of both models. At the outflow, a stress-free condition was assumed. No-slip conditions for the flow and fixed oxygen concentration (Ma *et al.* 1997; Kaazempur-Mofrad & Ethier 2001; Tarbell 2003; Tada & Tarbell 2006; Zhang *et al.* 2007), $y_w = 0.0015$, were assumed at the wall for simplicity. While this is a first-order approximation, equivalent to decoupling the wall-side from the blood-side mass transfer (Ethier 2002), it will not affect qualitatively the *Sh* number distribution, although it does affect absolute values (Moore & Ethier 1997). Nevertheless, since the main focus of this work is to address the effect of three-dimensionality on the flow and mass transfer, we believe our conclusions will not be altered by this approximation. It is thought that neglecting the effect of unsteadiness will not qualitatively influence the WSS distribution (Myers *et al.* 2001). The effect of unsteadiness on the Sherwood number (*Sh*) is not obvious and needs to be investigated.

The results are presented in terms of WSS and Sherwood number, which represents the non-dimensional mass flux through the vessel walls and is estimated as

$$Sh = \frac{-\frac{\partial y}{\partial n} d}{y_i - y_w}, \tag{2.2}$$

where y is the oxygen mass fraction in the blood; y_i is the oxygen mass fraction at the inlet; y_w is the oxygen mass fraction at the wall; n is the local normal to the vessel wall; and d is the vessel diameter.

3. RESULTS AND DISCUSSION

3.1. Cylindrical bend

Figure 3 shows the WSS and *Sh* number patterns for model 1 along the inner and outer wall lines. In the region upstream of the bend, the WSS is constant and the *Sh* number is a decreasing function of the distance, according to the Graetz–Nusselt solution. As the flow enters the bend, the WSS shows a sharp maximum at the inner wall (figure 3*a*) and a minimum at the outer wall (figure 3*b*). These counter-intuitive peaks are caused by the sharp change of the vessel primary curvature in the transition from the straight section to the bend and can therefore be considered model artefacts for the purpose of this work. At the bend, the centrifugal forces, which push the fluid element outwards, cause a maximum at the outer wall (figure 3*b*) and a minimum at the inner wall (figure 3*a*), which result in a large portion of the bend surface attaining WSS levels well above 1.5 Pa. The *Sh* number also peaks at the same locations, as a consequence of the convective effect, positive at the outer wall and has a minimum at the inner one, as a result of the displacement of oxygen-poor fluid from the outer wall to the inner one.

The WSS extremes are followed by a sharp decay, possibly owing to flow readjustment, which brings the WSS and *Sh* number to a plateau lasting to the end of the bend. The succeeding extremes, a maximum for the outer wall and a minimum for the inner wall, are caused by the end of the bend/beginning of the straight section, which produces a localized sharp change of the primary curvature. At the bend, the maximum to minimum WSS and *Sh* number ratios are approximately 5 and 29, respectively. As the flow enters the straight section downstream of the bend, the WSS tends to lower values at the outer wall and higher values at the inner wall, as the flow tends to adjust to its fully developed state in a straight vessel. The *Sh* number at the inner wall is consistently smaller, from 10 to 5 times, than at the outer wall. Also, its value at the inner wall does not change from the beginning of the bend to the end of the straight section, indicating that the oxygen distribution induced by the Dean vortices at the bend survives longer after the vortices have been dissipated. Figures 4*a* and 5*a* show the in-plane streamlines superimposed on the velocity magnitude iso-contours and the corresponding oxygen concentration iso-contours in figures 4*b* and 5*b* after the beginning of the bend (figure 4) and halfway to the end

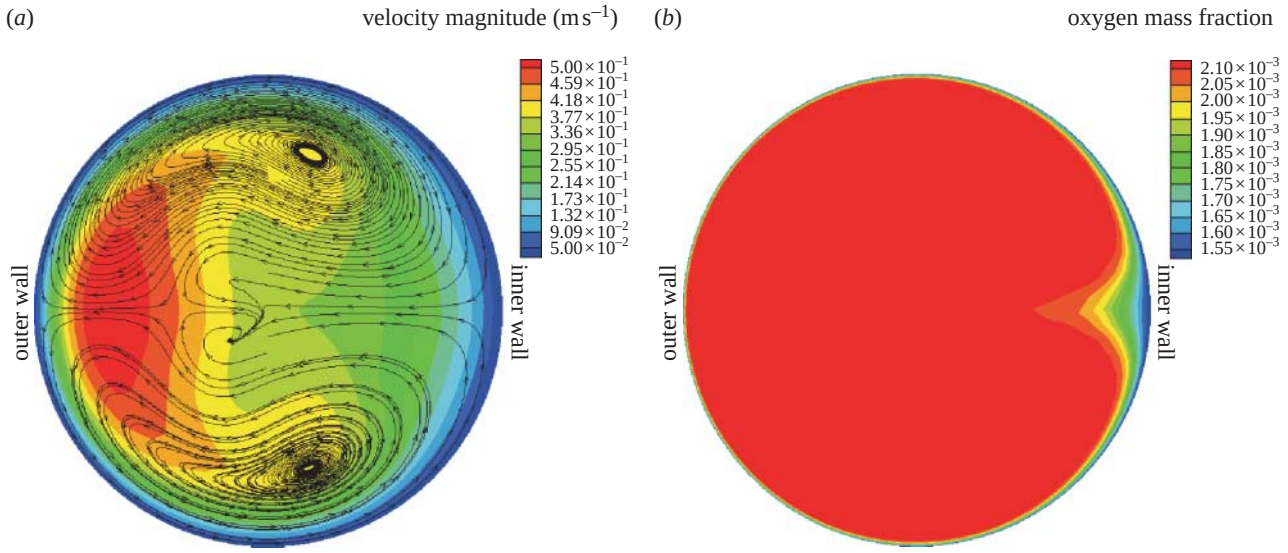

Figure 5. (*a*) Velocity magnitude iso-contours and in-plane streamlines; (*b*) oxygen iso-contours at a section 28*D* from the inlet in model 1 (about the bend mid-section). The inner and outer walls are also indicated.

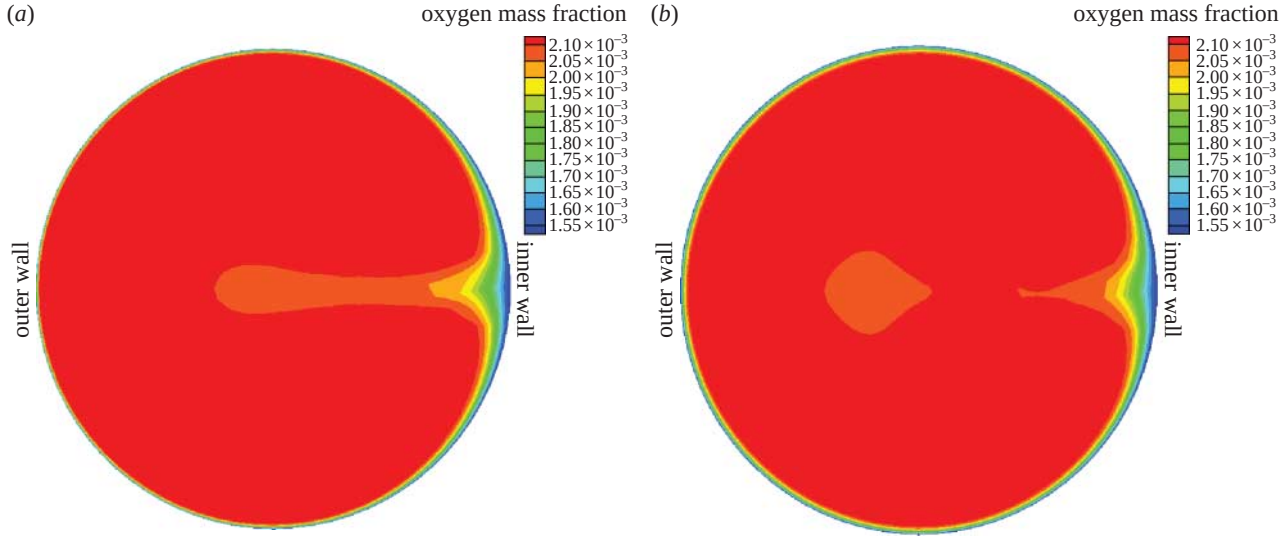

Figure 6. Oxygen iso-contours at a section (*a*) 33*D* and (*b*) 39*D* from the inlet in model 1. The inner and outer walls are also indicated.

of it (figure 5). The velocity and concentration profiles become skewed as the flow enters the bend (figure 4), as a consequence of the centrifugal forces, which push the fluid elements away from the inner wall towards the outer wall, generating two Dean vortices, as indicated by the superimposed streamlines in figure 4. This process continues throughout the bend, displacing low oxygen fluid away from the outer wall, along the sidewalls and bringing it towards the inner wall, producing a localized region with a thicker boundary layer (figure 5*b*).

After the bend, the Dean vortices lose intensity and move towards the centre, now bringing fluid with high oxygen concentration into the low-concentration patch. This process results in a detached region of low-concentration fluid at the centre and the low-concentration region at the wall (figure 6*b*), which will eventually disappear by diffusion. The oxygen distribution does not readjust as fast as the flow, as reflected by the different recovery rates of the WSS and *Sh* number (figure 3), and the overall result is a region where the physiological WSS is associated with a possible hypoxic condition, thus effectively uncoupling the effect of mass transport from WSS.

This is a very interesting result and, to the authors' knowledge, has not previously been reported in the literature, mainly because the existing literature is focused on the bend, disregarding the region downstream of it.

3.2. Helical bend

The *Sh* number and WSS distributions along the outer and inner wall lines versus the normalized axial distance are shown in figure 7. Figure 7*a*,*b* report the wall lines with respect to the primary curvature, while figure 7*c*,*d* report the profiles with respect to the secondary curvature. The *Sh* number and WSS profiles

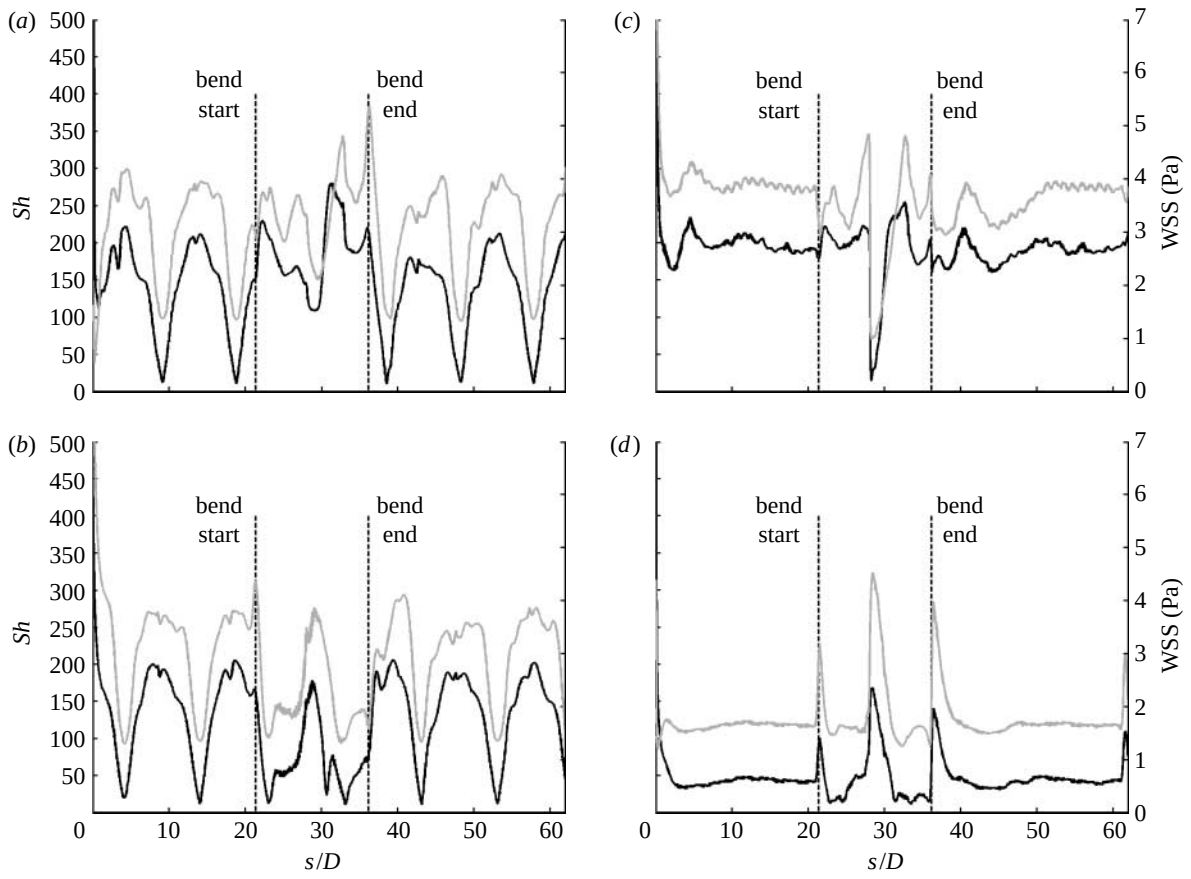

Figure 7. Sherwood number (black cuves) and WSS (grey curves) along (*a*,*c*) the outer (primary and secondary curvatures) and (*b*,*d*) inner (primary and secondary curvatures) wall lines of model 2 versus the axial distance from the inlet, normalized by the vessel diameter.

in all the plots of figure 7 show a high value at the inlet and a sharp decay. The high *Sh* number and WSS values at the inlet are a numerical artefact, caused by a slight misalignment between the inflow profile and the inflow cross section, with negligible effect on the overall results. The WSS and *Sh* number decay is instead caused by enhanced mixing induced by the centrifugal forces that act on the fluid elements soon after they enter the domain, as a consequence of geometry secondary curvature. It should be noted that in our model, the fully developed helical inflow condition itself introduces secondary motion, although this would develop with any inlet condition, given a sufficient entry length.

The primary curvature-based WSS and *Sh* number profiles (figure 7*a*,*b*) show an almost periodic pattern of maxima and minima, qualitatively similar to those found for a coronary artery (Kaazempur-Mofrad & Ethier 2001; Myers *et al.* 2001).

This pattern is clearly caused by the rotation of the Dean vortices, induced by the secondary curvature of the helix. In fact, the same pattern is absent in figure 7*c*,*d*, since the wall lines relative to the secondary curvature follow a helical pattern. Different from Myers's work is the origin of the vortices, here to be attributed solely to the secondary curvature. This is also an interesting result, since it implies that a coronary artery can potentially be described by a simple ideal model. At the bend, the outer wall lines show four peaks, while the inner wall lines show one narrow peak with lower maxima. This probably indicates that the bend in the medial plane is, overall, still displacing the high-concentration fluid towards the outer wall, but is not preventing the secondary curvature from inducing secondary flows and rotation. After the bend, the pattern is again almost periodic with *Sh* number and WSS patterns very similar to those in the section upstream of the bend suggesting that the flow has adjusted to the geometry.

The profiles based on the secondary curvature (figure 7*c*,*d*) show quite a different picture, as they are both relatively flat after the inlet section, up to the bend, in agreement with Tiwari *et al.* (2006). The wiggles found on the outer wall line (figure 7*c*) are data processing artefacts and do not affect our conclusions. There is a clear distinction between the bend section and the sections upstream and downstream of it. At the bend, the outer wall lines show a sharp minimum, while the inner wall lines have three sharp maxima, at the beginning, halfway and at the end of the bend. This can be better explained by looking at figures 8 and 9, showing velocity magnitude and concentration iso-contours at different cross sections throughout the bend and also some pathlines. The velocity profile is skewed as it enters the bend, with the high-velocity region closer to the outer wall, while the oxygen profile shows a low-concentration region on the inner wall.

The overall clockwise flow rotation, induced by the secondary curvature, allows the fluid elements to follow a smoother path through the first part of the bend, but skewing the velocity profile towards the top surface. In

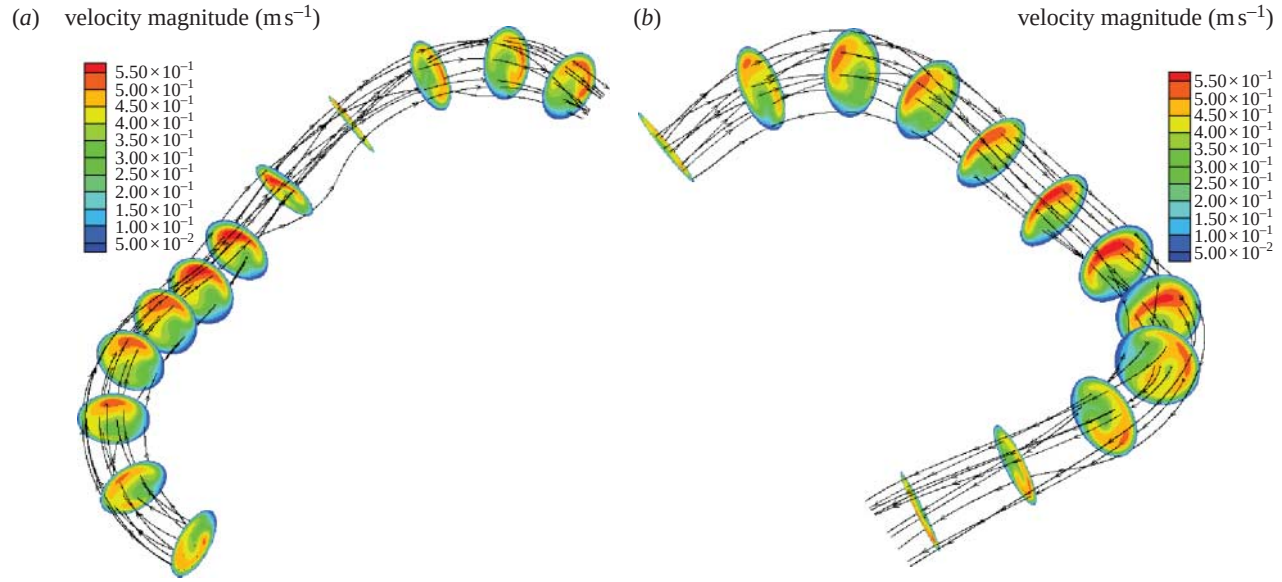

Figure 8. Velocity magnitude iso-contours and pathlines at the bend in model 2 from (*a*,*b*) two different angles of view. Flow is clockwise, from left to right.

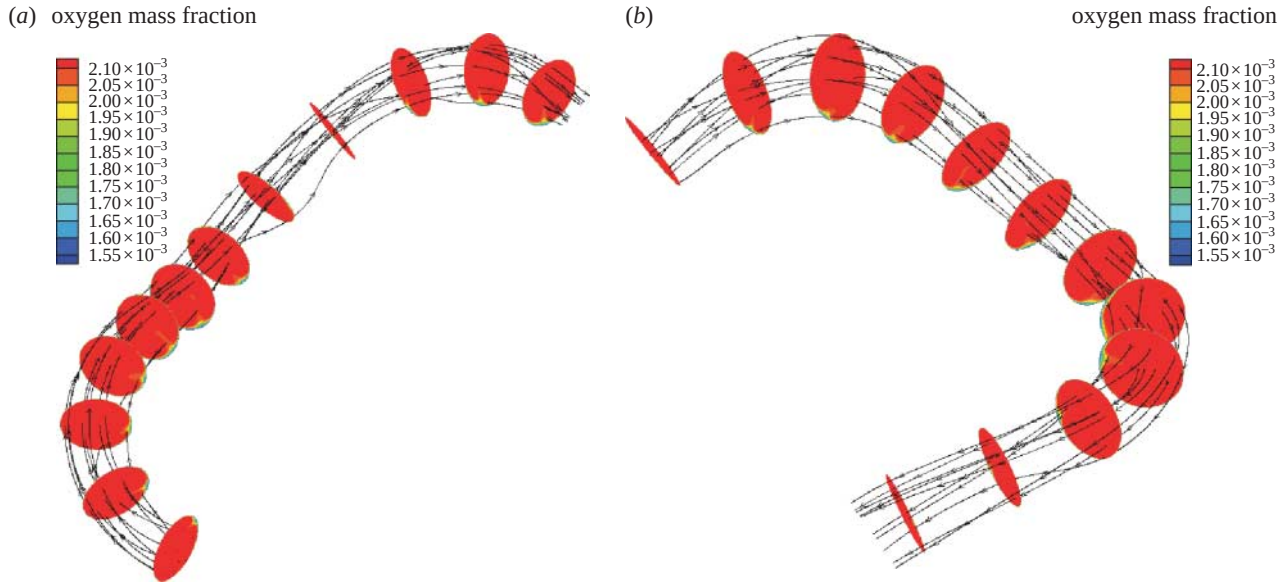

Figure 9. Oxygen iso-contours and pathlines at the bend in model 2 at (*a*,*b*) two different angles of view. Flow is clockwise, from left to right.

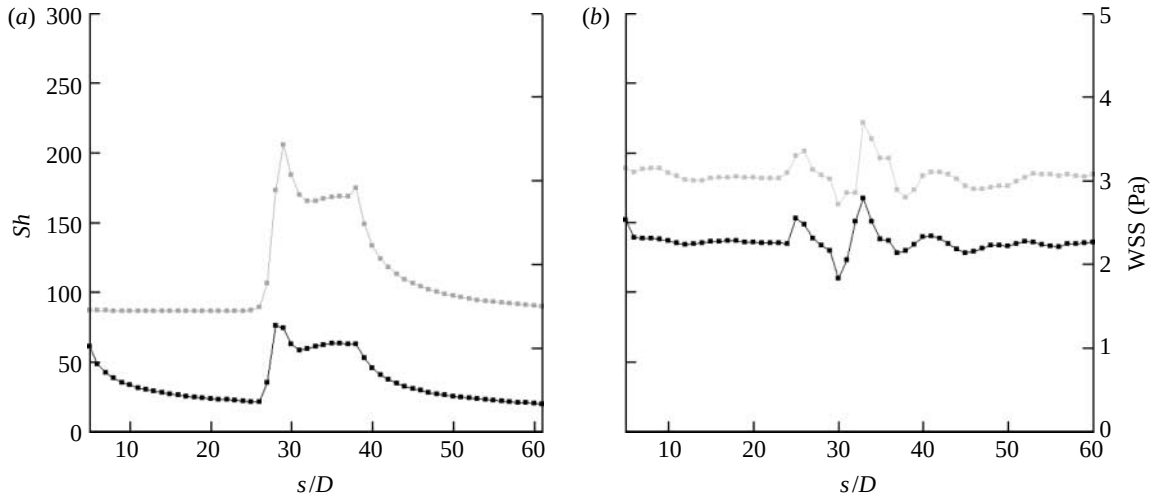

Figure 10. (*a*) Model 1 and (*b*) model 2 averaged *Sh* number (black filled squares) and WSS (grey filled squares) versus the axial distance from the inlet, normalized by the vessel diameter. The values have been averaged over the cross-sectional perimeters.

the second half of the bend, where the fluid is forced into a small anticlockwise rotation, the velocity profile undergoes a sharp change and the low oxygen region is spread along the inner wall, as shown in figures 8*b* and 9*b*. The sudden thinning of the oxygen boundary layer produces the spike in *Sh* number at the inner wall. Reverting to figures 6 and 7, we can see that this effect is almost unnoticeable following the primary curvature profiles, as it is embedded in the quasi-periodic pattern. At the bend, the maximum to minimum WSS and *Sh* number ratios are approximately 6 and 27, respectively. In the downstream section, the distributions appear very similar to those in the upstream section, with similar levels of *Sh* number, both at the outer and inner walls (figure 7), as a result of the flow adapting to the new configuration.

For an overall comparison between the two models, we computed, at each axial position, the circumferential average of the *Sh* number and WSS and plotted them in figure 10. The most noticeable features are the average values of WSS and *Sh* number throughout model 2, which are approximately two and four times, respectively, the equivalent values in model 1 and the reduced extremes attained at the bend in model 2 compared with model 1, suggesting that the area over which the extremes of *Sh* number and WSS are distributed is smaller in model 2 than in model 1.

4. CONCLUSIONS

In this work, we have studied computationally the effect of cross mixing on *Sh* number and WSS distributions, by comparing the findings in two well-defined geometries, a cylindrical and a helical U-bend.

The results suggest that WSS and mass transport can be uncoupled downstream of planar bends, opening the way to well-characterized experimental models to investigate the separate effect of WSS and oxygen supply.

We have shown that the helical geometry can be used as an idealized model capable of reproducing results from a realistic human coronary artery (Kaazempur-Mofrad & Ethier 2001), providing at the same time a simpler framework for understanding the effect of the geometrical parameters of the vessels. The model was not optimized for this study and, therefore, the level of qualitative agreement can be considered remarkable. The present work suggests that the WSS and *Sh* number patterns found in the coronary artery are a consequence of flow rotation (Kaazempur-Mofrad & Ethier 2001), but the cross-flow velocities are induced by the secondary curvature. Our results suggest that the maximum to minimum WSS and *Sh* number ratios are approximately 5 and 29, respectively, for the cylindrical geometry and 6 and 27 for the helical one, while the corresponding values found in Kaazempur-Mofrad & Ethier (2001) are 8 and 54.

The non-dimensional oxygen consumption rate in the tissue (Tarbell 2003) $\mathrm{Da} = QTD_{\mathrm{i}}/K\mathfrak{D}P_{\mathrm{b}} \sim 23$, where Q is the tissue consumption rate; T is the wall thickness; K is Henry's law constant; $\mathfrak{D}$ is the oxygen diffusivity; and P_{b} is the oxygen partial pressure. Here we assumed $T \sim 0.075$ cm (Fayad *et al.* 2000) and $Q/K\mathfrak{D} \sim 1.29 \times 10^5$ torr cm^{-2} (Tarbell 2003). Our simulations show that in model 1 the lowest $Sh \sim 5$, while in model 2 the lowest $Sh \sim 12$, and accounting for a 2.5 correction factor for neglecting haemoglobin (Moore & Ethier 1997), they would be 12.5 and 30, respectively, suggesting that the flux near the inner curvature of model 1 is fluid controlled, whereas in model 2 the flux is not fluid controlled.

We conclude that secondary motion resulting from three-dimensional geometry can appreciably influence the distribution of both the WSS and the Sherwood number. There is extensive study of the effects of WSS on vascular biology (Davies 1995; Gimbrone 1999; Himburg *et al.* 2004). Atherosclerosis is widely believed to develop in arteries where WSS is low (Caro *et al.* 1971; Giddens 1995; Malek *et al.* 1999) but the association between WSS and atherosclerosis may also depend on other factors, such as diet, blood lipid values, hypertension, diabetes and smoking.

Mixing and secondary motion within an artery may influence the blood–wall mass transport of oxygen and other low-molecular-weight species (Davies 1995). In addition, concentration polarization of macromolecules has been reported in arteries (Caro *et al.* 1985; Wada & Karino 2002). As a result, the equilibrium concentration of macromolecules at the blood–wall interface will be determined by factors including the convection of solvent through the wall and mixing within the vessel lumen. It is permissible to speculate, therefore, that mixing resulting from vessel three-dimensionality will also influence the concentration of macromolecules at the blood–wall interface and hence potentially macromolecule concentration within the wall. The study may assist in the experimental investigation of the influence of WSS and the mass transport of low- and high-molecular-weight species on vessel biology.

A number of workers have contributed in various ways to this study. They include Dr Peter Franke, Mr Jim Shaikh and Dr Stephanie Cremers. The work was supported by the Henry Smith Charity, the Clothworkers' Foundation and the Garfield Weston Foundation.

REFERENCES

Caro, C. G., Fitz-Gerald, J. M. & Schroter, R. C. 1971 Atheroma and arterial wall shear observation, correlation and proposal of a shear dependent mass transfer mechanism for altherogenesis. *Proc. R. Soc. B* **177**, 109–133. (doi:10.1098/rspb.1971.0019)

Caro, C. G., Lever, M. J. & Tarbell, J. M. 1985 Effect of luminal flow-rate on transmural fluid flux in the perfused rabbit common carotid-artery. *J. Physiol. Lond.* **365**, 92.

Caro, C. G., Doorly, D. J., Tarnawski, M., Scott, K. T., Long, Q. & Dumoulin, C. L. 1996 Non-planar curvature and branching of arteries and non-planar-type flow. *Proc. R. Soc. A* **452**, 185–197. (doi:10.1098/rspa.1996.0011)

Caro, C. G., Watkins, N., Doorly, D. J., Sherwin, S. J. & Peiró, J. 1998 Influence of non-planar geometry on flow separation. *J. Physiol.* **513**, 2P.

Caro, C. G., Cheshire, N. J. & Watkins, N. 2005 Preliminary comparative study of small amplitude helical and conventional ePTFE arteriovenous shunts in pigs. *J. R. Soc. Interface* **2**, 261–266. (doi:10.1098/rsif.2005.0044)

Caro, C. G., Cheshire, N., Ellis, D., Cerini, M. & Cremers, S. 2006 Implications of 3D vascular geometry. In *Keynote Lecture, 5th World Congress of Biomechanics, 29 July 2006.*

Davies, P. F. 1995 Flow-mediated endothelial mechanotransduction. *Physiol. Rev.* **75**, 519–560.

Dimmeler, S., Haendeler, J., Rippmann, V., Nehls, M. & Zeiher, A. M. 1996 Shear stress inhibits apoptosis of human endothelial cells. *FEBS Lett.* **399**, 71–74. (doi:10.1016/S0014-5793(96)01289-6)

Ethier, C. R. 2002 Computational modeling of mass transfer and links to atherosclerosis. *Ann. Biomed. Eng.* **30**, 461–471. (doi:10.1114/1.1468890)

Fayad, Z. A., Fuster, V., Fallon, J. T., Jayasundera, T., Worthley, S. G., Helft, G., Aguinaldo, J. G., Badimon, J. J. & Sharma, S. K. 2000 Noninvasive *in vivo* human coronary artery lumen and wall imaging using black-blood magnetic resonance imaging. *Circulation* **102**, 506–510.

Frazin, L., Lanza, G., Mehlman, D., Chandran, K. B., Vonesh, M., Spitzzeri, C., Mcgee, S., Talano, J. & Mcpherson, D. 1990 Rotational blood-flow in the thoracic aorta. *Clin. Res.* **38**, A331.

Friedman, M. H. & Ding, Z. H. 1998 Relation between the structural asymmetry of coronary branch vessels and the angle at their origin. *J. Biomech.* **31**, 273–278. (doi:10.1016/S0021-9290(98)00013-X)

Giddens, D. P. 1995 *Fluid dynamics of end-to-side vascular grafts*. New York, NY: Plenum Publishing Corporation.

Gimbrone, M. A. 1999 Vascular endothelium, hemodynamic forces, and atherogenesis. *Am. J. Pathol.* **155**, 1–5.

Himburg, H. A., Grzybowski, D. M., Hazel, A. L., Lamack, J. A., Li, X. M. & Friedman, M. H. 2004 Spatial comparison between wall shear stress measures and porcine arterial endothelial permeability. *Am. J. Physiol. Heart Circ. Physiol.* **286**, H1916–H1922. (doi:10.1152/ajpheart.00897.2003)

Huijbregts, H. J. T. A., Blankestijn, P. J., Caro, C. G., Cheshire, N. J. W., Hoedt, M. T. C., Nolthenius, R. P. T. & Moll, F. L. 2007 A helical PTFE arteriovenous access graft to swirl flow across the distal anastomosis: results of a preliminary clinical study. *Eur. J. Vasc. Endovasc. Surg.* **33**, 472–475. (doi:10.1016/j.ejvs.2006.10.028)

Kaazempur-Mofrad, M. R. & Ethier, C. R. 2001 Mass transport in an anatomically realistic human right coronary artery. *Ann. Biomed. Eng.* **29**, 121–127. (doi:10.1114/1.1349704)

Kaazempur-Mofrad, M. R., Wada, S., Myers, J. G. & Ethier, C. R. 2005 Mass transport and fluid flow in stenotic arteries: axisymmetric and asymmetric models. *Int. J. Heat Mass Transfer* **48**, 4510–4517. (doi:10.1016/j.ijheatmasstransfer.2005.05.004)

Kamiya, A., Bukhari, R. & Togawa, T. 1984 Adaptive regulation of wall shear-stress optimizing vascular tree function. *Bull. Math. Biol.* **46**, 127–137.

Langille, B. L. & O'Donnell, F. 1986 Reductions in arterial diameter produced by chronic decreases in blood-flow are endothelium-dependent. *Science* **231**, 405–407. (doi:10.1126/science.3941904)

Liu, S. J. & Masliyah, J. H. 1993 Axially invariant laminar-flow in helical pipes with a finite pitch. *J. Fluid Mech.* **251**, 315–353. (doi:10.1017/S002211209300343X)

Long, Q., Xu, X. Y., Ariff, B., Thom, S. A., Hughes, A. D. & Stanton, A. V. 2000 Reconstruction of blood flow patterns in a human carotid bifurcation: a combined CFD and MRI study. *J. Magn. Reson. Imaging* **11**, 299–311. (doi:10.1002/(SICI)1522-2586(200003)11:3<299::AID-JMRI9>3.0.CO;2-M)

Ma, P. P., Li, X. M. & Ku, D. N. 1997 Convective mass transfer at the carotid bifurcation. *J. Biomech.* **30**, 565–571. (doi:10.1016/S0021-9290(97)84506-X)

Malek, A. M., Alper, S. L. & Izumo, S. 1999 Hemodynamic shear stress and its role in atherosclerosis. *J. Am. Med. Assoc.* **282**, 2035–2042. (doi:10.1001/jama.282.21.2035)

Moore, J. A. & Ethier, C. R. 1997 Oxygen mass transfer calculations in large arteries. *J. Biomech. Eng. Trans. ASME* **119**, 469–475.

Myers, J. G., Moore, J. A., Ojha, M., Johnston, K. W. & Ethier, C. R. 2001 Factors influencing blood flow patterns in the human right coronary artery. *Ann. Biomed. Eng.* **29**, 109–120. (doi:10.1114/1.1349703)

O'Flynn, P. M., O'Sullivan, G. & Pandit, A. S. 2007 Methods for three-dimensional geometric characterization of the arterial vasculature. *Ann. Biomed. Eng.* **35**, 1368–1381. (doi:10.1007/s10439-007-9307-9)

Palumbo, R., Gaetano, C., Antonini, A., Pompilio, G., Bracco, E., Ronnstrand, L., Heldin, C. H. & Capogrossi, M. C. 2002 Different effects of high and low shear stress on platelet-derived growth factor isoform release by endothelial cells—consequences for smooth muscle cell migration. *Arterioscler. Thromb. Vasc. Biol.* **22**, 405–411. (doi:10.1161/hq0302.104528)

Perktold, K., Leuprecht, A., Prosi, M., Berk, T., Czerny, M., Trubel, W. & Schima, H. 2002 Fluid dynamics, wall mechanics, and oxygen transfer in peripheral bypass anastomoses. *Ann. Biomed. Eng.* **30**, 447–460. (doi:10.1114/1.1477445)

Qiu, Y. C. & Tarbell, J. M. 2000 Numerical simulation of oxygen mass transfer in a compliant curved tube model of a coronary artery. *Ann. Biomed. Eng.* **28**, 26–38. (doi:10.1114/1.251)

Stonebridge, P. A. & Brophy, C. M. 1991 Spiral laminar-flow in arteries? *Lancet* **338**, 1360–1361. (doi:10.1016/0140-6736(91)92238-W)

Stonebridge, P. A., Hoskins, P. & Allan, P. 1994 *In-vivo* stable spiral laminar-flow. *Br. J. Surg.* **81**, 613.

Tada, S. & Tarbell, J. M. 2006 Oxygen mass transport in a compliant carotid bifurcation model. *Ann. Biomed. Eng.* **34**, 1389–1399. (doi:10.1007/s10439-006-9155-z)

Tarbell, J. M. 2003 Mass transport in arteries and the localization of atherosclerosis. *Annu. Rev. Biomed. Eng.* **5**, 79–118. (doi:10.1146/annurev.bioeng.5.040202.121529)

Tiwari, P., Antal, S. P. & Podowski, M. Z. 2006 Three-dimensional fluid mechanics of particulate two-phase flows in U-bend and helical conduits. *Phys. Fluids* **18**, 043 304. (doi:10.1063/1.2189212)

Wada, S. & Karino, T. 2002 Theoretical prediction of low-density lipoproteins concentration at the luminal surface of an artery with a multiple bend. *Ann. Biomed. Eng.* **30**, 778–791. (doi:10.1114/1.1495868)

Wood, N. B., Zhao, S. Z., Zambanini, A., Jackson, M., Gedroyc, W., Thom, S. A., Hughes, A. D. & Xu, X. Y. 2006 Curvature and tortuosity of the superficial femoral artery: a possible risk factor for peripheral arterial disease. *J. Appl. Physiol.* **101**, 1412–1418. (doi:10.1152/japplphysiol.00051.2006)

Zabielski, L. & Mestel, A. J. 1998 Steady flow in a helically symmetric pipe. *J. Fluid Mech.* **370**, 297–320. (doi:10.1017/S0022112098002006)

Zhang, Z. G., Fan, Y. B. & Deng, X. Y. 2007 Oxygen transfer in human carotid artery bifurcation. *Acta Mech. Sin.* **23**, 305–309. (doi:10.1007/s10409-007-0080-7)